

# Continual Learning in 3D Point Clouds: Employing Spectral Techniques for Exemplar Selection

Hossein Resani, Behrooz Nasihatkon, Mohammadreza Alimoradi Jazi  
K. N. Toosi University of Technology

## Abstract

We introduce a novel framework for *Continual Learning in 3D object classification (CL3D)*. Our approach is based on the selection of prototypes from each class using spectral clustering. For non-Euclidean data such as point clouds, spectral clustering can be employed as long as one can define a distance measure between pairs of samples. Choosing the appropriate distance measure enables us to leverage 3D geometric characteristics to identify representative prototypes for each class. We explore the effectiveness of clustering in the input space (3D points), local feature space (1024-dimensional points), and global feature space. We conduct experiments on the ModelNet40, ShapeNet, and ScanNet datasets, achieving state-of-the-art accuracy exclusively through the use of input space features. By leveraging the combined input, local, and global features, we have improved the state-of-the-art on ModelNet and ShapeNet, utilizing nearly half the memory used by competing approaches. For the challenging ScanNet dataset, our method enhances accuracy by 4.1% while consuming just 28% of the memory used by our competitors, demonstrating the scalability of our approach. The code will be made publicly available.

## 1. Introduction

In recent years, deep learning for point cloud processing has become a key focus in computer vision research due to its wide range of applications [18, 49]. However, much of the progress has been made under idealized conditions. In real-world applications, gathering data for all object classes simultaneously is often impractical. Typically, models are initially trained on a large dataset for specific classes, known as the base task, to develop a baseline model. As new data for additional classes—referred to as novel tasks—becomes available, the model needs to be updated incrementally. However, retraining the model with

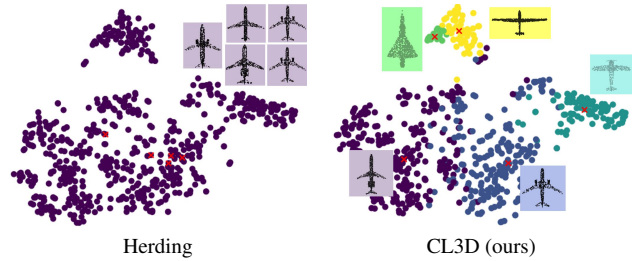


Figure 1. t-SNE visualization of global features of the airplane class and exemplars selected by the *herding* approach [36] (left) contrasted with those from our CL3D method (right). Different colors denote different clusters. Our method effectively covers different subcategories of the airplane samples, demonstrating improved exemplar selection compared to the herding approach.

both base and novel data is often not feasible due to hardware limitations or privacy concerns. This leads to the problem of *catastrophic forgetting* [22], where the model loses its ability to recognize previously learned classes when adapting to new ones. Continual learning offers a solution by enabling models to learn from new data while retaining knowledge of prior tasks, which is critical for adaptive applications. While continual learning has been extensively studied for 2D images, its application to 3D point cloud data remains largely underexplored.

3D data representation poses significant challenges compared to 2D data due to the irregular structure of point clouds, which lack the uniformity of pixel grids in images. This makes it difficult to apply traditional CNNs, which are designed for structured data like pixel grids. Instead, specialized techniques such as PointNet [33], PointNet++ [34], and graph neural networks [39, 43, 51] are used to handle the 3D data. Additionally, the 3D domain suffers from resource scarcity and limited datasets, with ModelNet40 [47] being significantly smaller and less diverse than 2D datasets like ImageNet [12]. This limitation hampers the ability of 3D models to learn robust and distinct features, complicating classification tasks. [8, 18, 52]

The unique characteristics of 3D point clouds directly affect the performance of memory-based continual learning methods, where a few exemplars from old classes are stored to aid future learning stages. Traditional exemplar selection methods, such as *herding* [36], become ineffective due to the irregular and multimodal nature of 3D feature spaces. Moreover, exemplar selection must consider the geometry and structural properties specific to point clouds to be effective. Fig. 1 provides an illustration of this phenomenon.

To address these challenges, we propose a novel method for exemplar selection that leverages the geometry of input point clouds through spectral clustering, which is well-suited for non-Euclidean data. Additionally, we extend this approach to perform clustering on local features and employ k-means clustering for global features. Our contributions include:

- **Clustering-based Exemplar Selection:** We demonstrate that clustering for exemplar selection in 3D point clouds, whether applied to input point clouds, local features, or global features, is much more effective than traditional approaches such as *herding* [36].
- **Geometry-Aware Exemplar Selection:** We introduce an exemplar selection method based on spectral clustering that utilizes the intrinsic geometric properties of 3D point clouds, independent of the backbone architecture. We further extend this to perform clustering on local features.
- **Fusing Clustering Domains:** We present an innovative approach to fuse embeddings from the input space, local feature space, and global feature space to enhance exemplar selection via clustering.
- **State-of-the-Art Performance:** Our method achieves state-of-the-art results on three prominent point cloud benchmarks: ModelNet40 [47], ShapeNet [5], and ScanNet [11]. Averaged over incremental stages, our method surpasses previous state-of-the-art methods by 3.4%, 2%, and 4.1% on ModelNet40, ShapeNet, and ScanNet, respectively, while requiring fewer exemplars in memory. Notably, in the final incremental stage, these improvements are astonishing, reaching 16.9%, 3.0%, and 14.0% on ModelNet40, ShapeNet, and ScanNet, respectively.

## 2. Related Work

### 2.1. Point Cloud Classification

PointNet [33] utilizes max-pooling to provide permutation-invariant features suitable for classification tasks. Subsequent studies [34, 35, 43, 48, 50] have developed various architectures to compile information from points nearby, although many continue to use

max-pooling to achieve permutation invariance. These techniques are collectively known as point-based methods. In contrast, some techniques [17, 24] transform 3D point clouds into 2D image representations, applying traditional image processing techniques for predictions.

### 2.2. Continual Learning on 2D Images

The issue of catastrophic forgetting [30] has been a focal point of research. Existing literature typically falls into one of three categories: memory-based [4, 20, 32, 36, 40, 44], regularization-based [7, 13, 25, 54], and parameter isolation-based strategies [27, 28, 37]. Memory-based approaches maintain or recreate exemplars from past tasks to integrate with new task training, or alternatively, generate new examples for this purpose. Parameter isolation techniques dedicate certain parameters exclusively to each task to minimize forgetting. Regularization strategies are divided into those that are prior-focused, which view knowledge as the values of parameters and restrict new task learning by penalizing significant alterations to parameters critical for previous tasks [1, 7, 54], and those that are data-focused, which leverage knowledge distillation [19] by applying a regularization term based on the discrepancy between activations of the old and new networks to mitigate catastrophic forgetting [13, 25].

### 2.3. Continual Learning on 3D Point Cloud

While continual learning has seen significant progress in 2D, the 3D domain remains underdeveloped. Chowdhury *et al.* [10] used knowledge distillation and semantic word vectors to reduce catastrophic forgetting. Zhao *et al.* [55] addressed this issue in 3D object detection with static and dynamic teachers. Zamorski *et al.* [53] introduced Random Compression Rehearsal (RCR), using a compact model to compress and store key data from previous tasks.

Several studies align with our work. Chowdhury *et al.* [9] propose using Microshapes—orthogonal basis vectors to represent 3D objects, which help bridge the gap between synthetic and real data, improving model robustness against noise. I3DOL [14] addresses irregular point cloud data with an adaptive-geometric centroid module and a geometric-aware attention mechanism to focus on key local structures and reduce forgetting. It also introduces a score fairness compensation strategy to balance training between new and old classes. InOR-Net [15] enhances this approach with *category-guided geometric reasoning* and *critic-induced geometric attention* to identify key 3D features. It also introduces a dual adaptive fairness compensation strategy to address class imbalances and avoid biased predictions. While these methods rely on the herding algorithm designed for 2D image data, we employ a different exemplar selection strategy that is more effective for 3D point clouds.

### 3. Background

Consider a sequence of disjoint tasks  $\mathcal{D} = \{\mathcal{D}^1, \dots, \mathcal{D}^T\}$ , where  $\mathcal{C}^t = \{c_1^t, \dots, c_{m_t}^t\}$  is the set of classes in the task  $\mathcal{D}^t$ . Note that the classes between all tasks are disjoint, i.e.,  $\mathcal{C}^i \cap \mathcal{C}^j = \emptyset, \forall i, j \in \{1, \dots, T\}$ , where  $i \neq j$ . The goal of continual learning is to progressively train a model, where at each stage  $t$ , only the training samples from the current task  $\mathcal{D}^t = X^t, Y^t$ , consisting of point clouds  $X^t$  and their corresponding labels  $Y^t$ , are accessible. During testing, the model trained on task  $\mathcal{D}^t$  is expected to predict outputs not only for the current task but also for all prior tasks, i.e.,  $\{\mathcal{D}^1, \dots, \mathcal{D}^{t-1}\}$ .

#### 3.1. Memory-based Continual Learning

In *memory-based* continual learning, we maintain a memory  $M$  of *exemplars*, which are selected samples from previous tasks to represent old classes.

For a newly trained feature extractor  $f_t$  on new data and the previous feature extractor  $f_{t-1}$ , we use old class prototypes up to task  $t - 1$ . To update  $M$  after each task, a common strategy for selecting representative exemplars is the *herding* algorithm [36], which computes class centroids in feature space and selects exemplars based on their proximity to these centroids. The algorithm iteratively builds a memory  $M$  of representative samples closest to each centroid.

Nevertheless, herding faces limitations in 3D object domains due to the multi-modal distribution of each class in feature space [10]. In 3D point clouds, herding tends to select exemplars from a dominant mode, missing the diversity of the data. In contrast, our method selects exemplars from multiple modes, better capturing the complexity and variability of the data.

#### 3.2. PointNet

In this paper, we present our methodology within the framework of PointNet [33]. Similar adaptations may be made to other architectures. Let the  $i$ -th training sample be  $(X_i, y_i)$  where  $X_i \in \mathbb{R}^{n_i \times 3}$  is the  $i$ -th input point cloud and  $y_i \in \{1, \dots, C\}$  is the corresponding class label. Each row of  $X_i$  is a single 3D point in the point cloud. In a standard PointNet approach, each input point cloud  $X_i$  is processed as follows

1. First a shared MLP mapping  $f_\theta: \mathbb{R}^3 \rightarrow \mathbb{R}^F$  is applied to each row of  $X_i$ , resulting in a matrix  $Z_i \in \mathbb{R}^{n_i \times F}$ . The rows of  $Z_i$  can be considered as features local to each 3D point in the point cloud. Hence, they are referred to as *local features*. Notice that  $Z_i \in \mathbb{R}^{n_i \times F}$  can be viewed as a point cloud in  $\mathbb{R}^F$ .
2. Next, a pooling operator (usually max-pooling) is applied to the columns of  $Z_i \in \mathbb{R}^{n_i \times F}$  giving a *global feature*  $z_i \in \mathbb{R}^F$ .

3. Another MLP  $g_\phi: \mathbb{R}^F \rightarrow \mathbb{R}^C$  maps  $z_i$  to  $C$  classes.

The network parameters  $(\theta, \phi)$  may be learned via back-propagation using a standard cross-entropy loss.

### 4. Proposed Method

To perform memory-based continual learning, we choose  $K$  candidate exemplars from each old class to store in the memory. To do this, we divide the samples of each class into  $K$  clusters and choose a single exemplar per cluster. The clustering may be applied to the 3D input point clouds  $X_i$ , the local features  $Z_i$ , or the global features  $z_i$ . Due to their non-Euclidean nature, we perform a spectral embedding on  $X_i$ -s or  $Z_i$ -s before clustering. The global features  $z_i$  could be clustered with or without a spectral embedding. We also demonstrate that clustering is most effective when all these three domains are fused together. Our pipeline has been depicted in Fig. 2, and is detailed in the rest of this section.

#### 4.1. Spectral Clustering on Point Clouds

Spectral clustering [31,42] is known for its ability to handle complex non-Euclidean data. To apply it to 3D point clouds we need to define a measure of similarity or affinity between any pairs of point clouds. Let us restrict ourselves to a specific class with  $L$  data samples  $X_1, X_2, \dots, X_L$  with  $X_i \in \mathbb{R}^{n_i \times 3}$ . We form an affinity matrix  $A \in \mathbb{R}^{L \times L}$  representing the similarity between pairs of point clouds within this class, that is  $A_{ij} = \text{affinity}(X_i, X_j)$ . We will shortly discuss how to obtain this affinity measure. Having an affinity matrix, we form the normalized Laplacian matrix  $I - D^{-1/2} A D^{-1/2} \in \mathbb{R}^{L \times L}$  and compute its eigenvectors  $\mathbf{v}_1, \mathbf{v}_2, \dots, \mathbf{v}_K \in \mathbb{R}^L$  corresponding to the  $K$  smallest eigenvalues, where  $K$  is the intended number of clusters. The rows of the matrix  $V_{\text{input}} = [\mathbf{v}_1, \mathbf{v}_2, \dots, \mathbf{v}_K] \in \mathbb{R}^{L \times K}$  give an embedding of the *input* point cloud samples in  $\mathbb{R}^K$ . In fact, the  $i$ -th rows of  $V_{\text{input}} \in \mathbb{R}^{L \times K}$  is the input point cloud  $X_i \in \mathbb{R}^{n_i \times 3}$  embedded in this new space. One can cluster the data points into  $K$  categories by applying any Euclidean clustering approach such as *k-means* on the embedded data (rows of  $V_{\text{input}}$ ). Fig. 3 shows an example of applying spectral clustering on the *airplane* and *cup* datasets.

##### 4.1.1 Affinity Measure

Several methods can measure an affinity or, alternatively, a distance between a pair of point clouds [45]. Here, We select the Chamfer Distance (CD) [45] because it has a relatively lower computational cost compared to other distance metrics, such as the Earth Mover's Distance (EMD). Consider a pair of point clouds  $X_1 \in \mathbb{R}^{n_1 \times 3}$  and  $X_2 \in \mathbb{R}^{n_2 \times 3}$  and let  $\mathbf{x}_1^i, \mathbf{x}_2^i \in \mathbb{R}^3$  be the  $i$ -th rows of  $X_1$  and  $X_2$ , respectively. First we register the point clouds to align together.

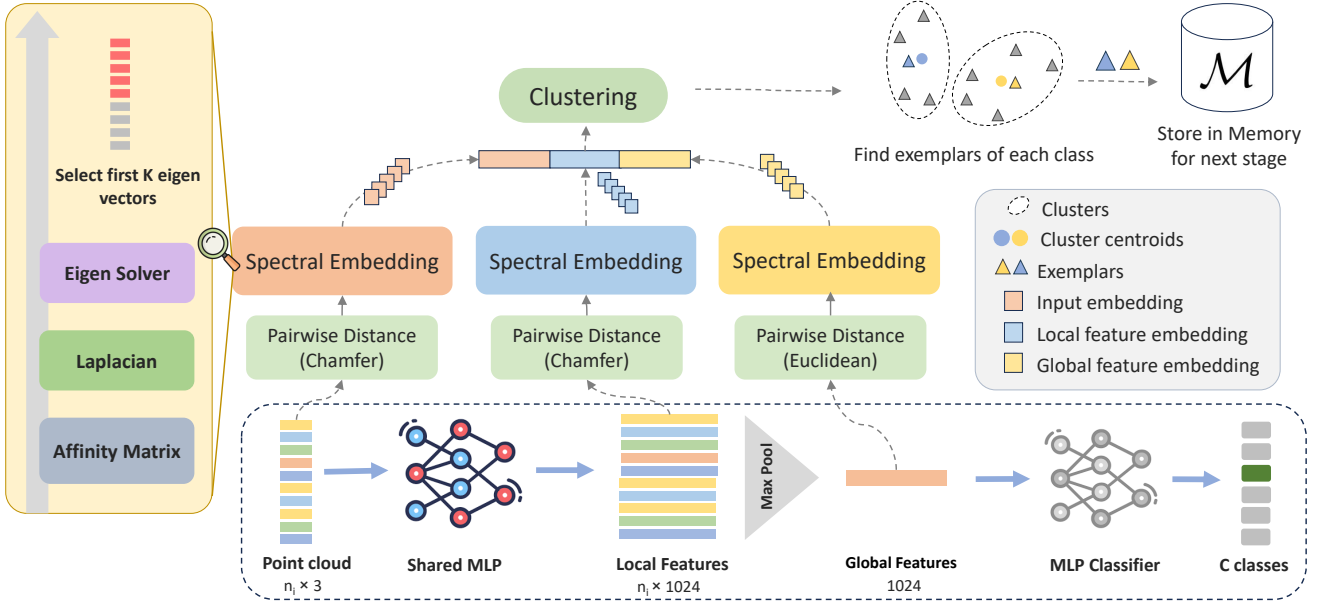


Figure 2. Overview of CL3D training pipeline. Spectral embeddings may be computed from the input, the local features, and the global features. They can be simply fused together by concatenation and fed to  $k$ -means for clustering. Finally, the class exemplars are selected based on proximity to each cluster’s centroid.

Then, we find a mapping from each point  $\mathbf{x}_1^i$  in  $X_1$  to its closest point in  $X_2$  and vice versa:

$$j_i^* = \operatorname{argmin}_j \|\mathbf{x}_1^i - \mathbf{x}_2^j\|, \quad i_j^* = \operatorname{argmin}_i \|\mathbf{x}_1^i - \mathbf{x}_2^j\|. \quad (1)$$

The Chamfer distance is then defined as the average distance of each point in one point cloud to its nearest point in the other point cloud:

$$\begin{aligned} \text{CD}(X_1, X_2) &= \frac{1}{n_1} \sum_{i=1}^{n_1} \|\mathbf{x}_1^i - \mathbf{x}_2^{j_i^*}\| \\ &+ \frac{1}{n_2} \sum_{j=1}^{n_2} \|\mathbf{x}_2^j - \mathbf{x}_1^{i_j^*}\|. \end{aligned} \quad (2)$$

Notice that, like most distance measures on point clouds, the above is only meaningful if the two shapes are aligned together. Various techniques exist for this, such as Iterative Closest Point (ICP) [2] and Fast Point Feature Histograms (FPFH) [38]. For some datasets such as ModelNet40 [47] the samples for each class are already aligned. For datasets lacking alignment, we employ FilterReg [16], a probabilistic registration method known for its robustness, precision, and efficiency. Notice that the alignment is solely conducted for exemplar selection. Once selected, the unaligned versions of the exemplars are added to the memory. The models are *trained and tested* on the unaligned point clouds.

It remains to form an affinity matrix from the distance matrix. Typically a radial basis kernel is used for this purpose. Here, we found that using the  $k$ -nearest neighbors

connectivity matrix for affinity improves the results. This means that, for each sample, the affinity is set equal to 1 for its  $k$  nearest neighbors and to 0 otherwise. We use  $k = 10$  in our experiments. The final affinity matrix is symmetrized as  $A \leftarrow (A + A^T)/2$ . final point is that calculating the affinity are not in the training process so they dont affect the traingin

#### 4.1.2 Exemplar Selection and Memory Management

Having segregated the data from each class into distinct clusters, we select, for every cluster, the sample nearest to its centroid in the embedded spectral space to serve as an exemplar. Within the context of continual learning, two primary memory management strategies are exercised: maintaining a fixed number of samples per class, or imposing a certain memory cap [29, 56]. Here, we opt for the first one.

#### 4.2. Clustering in Local Feature Space

Utilizing raw input data for clustering presents advantages such as simplicity, interpretability, efficiency, and independence from architectural constraints. However, as we move forward in the network the data should have better representational properties for the specific task at hand. This motivates us to apply spectral clustering on local features  $Z_i \in \mathbb{R}^{n_i \times F}$ . We anticipate improved results as moving closer to the feature space may result in representatives tailored for our specific task and the specific architecture being trained. Similar to PointNet [33] we choose  $F = 1024$ .



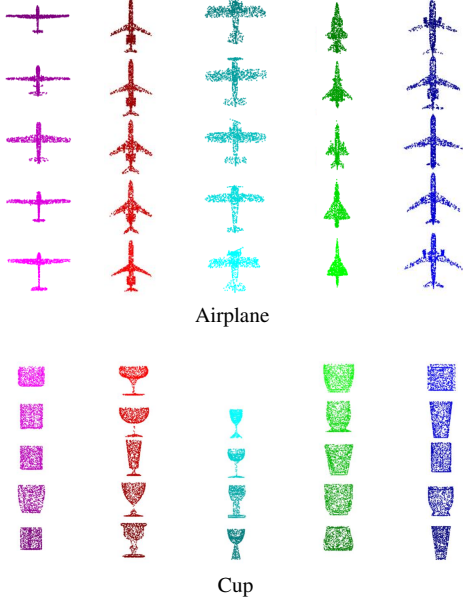


Figure 3. The output of spectral clustering in the input space for the *airplane* and *cup* classes in the ModelNet40 dataset. The different colors within each class represent different clusters.

Our model effectively distinguish the various subtypes of both airplanes and cups.

The main obstacle in applying spectral clustering in such a high-dimensional space is the time and memory complexity of the registration and computing the distance between pairs of point clouds. Remember that for computing the Chamfer distance one needs to align the point clouds and then for each point in one point cloud search for the nearest neighbor in the other. To circumvent these steps altogether, we use the nearest neighbor mappings (1) from the 3D point clouds  $X_i \in \mathbb{R}^{n_i \times 3}$  to compute the Chamfer distance in the  $F$ -dimensional point clouds  $Z_i \in \mathbb{R}^{n_i \times F}$ . In other words, for two sets of local features  $Z_1 \in \mathbb{R}^{n_1 \times F}$  and  $Z_2 \in \mathbb{R}^{n_2 \times F}$  the Chamfer distance is approximated as

$$\begin{aligned} \tilde{CD}(Z_1, Z_2) &= \frac{1}{n_1} \sum_{i=1}^{n_1} \|z_1^i - z_2^{j_i^*}\|_2 \\ &+ \frac{1}{n_2} \sum_{j=1}^{n_2} \|z_2^j - z_1^{i_j^*}\|_2. \end{aligned} \quad (3)$$

where the indices  $j_i^*$  and  $i_j^*$  are computed using (1) on the corresponding 3D point clouds  $X_1 \in \mathbb{R}^{n_1 \times 3}$  and  $X_2 \in \mathbb{R}^{n_2 \times 3}$ . Notice that, although the model has been trained with unaligned data, to use (3) we need to feed the network with aligned data. Of course, when exemplars are selected, their unaligned version is stored in the memory.

### 4.3. Clustering in Global Feature Space

As discussed in Sec. 3.2, max pooling transforms the local features  $Z_i \in \mathbb{R}^{n_i \times F}$  into a single  $F$ -dimensional vector  $z_i \in \mathbb{R}^F$ , designated as the *global feature*. Given their Euclidean nature, the  $K$ -means clustering can be straightforwardly applied to these global features. Alternatively, spectral clustering can be conducted using the Euclidean distance as a metric. Our experiments indicate that, when using global features alone,  $K$ -means clustering exhibits a slight advantage over spectral clustering.

### 4.4. Fusing Clustering Methods

To further improve performance, we propose a method that integrates the previously mentioned techniques. Our core strategy involves concatenating the embedded features from each technique and then executing clustering. Remember from Sec. 4.1 that for a certain class with  $L$  data samples  $X_1, X_2, \dots, X_L$ , spectral embedding results in a matrix  $V_{\text{input}} \in \mathbb{R}^{L \times K}$  where  $K$  is the intended number of clusters, and the  $i$ -th row of  $V$  is the embedding of  $X_i \in \mathbb{R}^{n_i \times 3}$  into  $\mathbb{R}^K$ . A similar matrix  $V_{\text{local}} \in \mathbb{R}^{L \times K}$  can be obtained for spectral embedding of the local features  $Z_1, Z_2, \dots, Z_L$ . To fuse the two methods we simply run  $K$ -means on the rows of their horizontal concatenation  $[V_{\text{input}}, V_{\text{local}}] \in \mathbb{R}^{L \times 2K}$ . This is straightforward due to the identical dimensions and similar scales of  $V_{\text{input}}$  and  $V_{\text{local}}$  stemming from their common basis in spectral analysis.

The main challenge arises when attempting to concatenate the 1024-dimensional global features  $z_1, z_2, \dots, z_L \in \mathbb{R}^F$  with these. Our findings suggest that direct concatenation of  $V_{\text{input}}$  and  $V_{\text{local}}$  with the matrix  $Z_{\text{global}} = [z_1, z_2, \dots, z_L]^T \in \mathbb{R}^{L \times F}$  leads to a decrease in accuracy, even after experimenting with various normalization techniques. To circumvent this, we apply spectral embedding to the global features using the conventional Euclidean metric to obtain  $V_{\text{global}} \in \mathbb{R}^{L \times K}$ . Now,  $V_{\text{global}}$  matches the size and scale of the vectors  $V_{\text{input}}$  and  $V_{\text{local}}$  allowing for an effective concatenation  $[V_{\text{input}}, V_{\text{local}}, V_{\text{global}}] \in \mathbb{R}^{L \times 3K}$ .

In Sec. 4.3, we noted that the spectral embedding of global features could degrade performance compared to applying  $K$ -means on the raw features. Nevertheless, we found this approach beneficial for merging methods. Our detailed analysis in Sec. 5.3 indicates that this holistic integration of all three methods outperforms the results of combining just two methods.

### 4.5. Class Imbalance Problem

A principal challenge in memory-based continual learning scenarios is the substantial imbalance between the exemplars of the previously learned classes and the samples of the newly introduced classes. Several strategies have been proposed to address this issue. For example, [41] utilizes a cosine distance metric to mitigate bias in the output

Incremental Stage	1	2	3	4	5	6	7	8	9	10	Avg.	$\Delta(\%)$	M
Number of Classes	4	8	12	16	20	24	28	32	36	40			
<i>joint</i>	98.5	99.3	98.2	95.8	96.4	94.4	91.9	91.5	90.6	88.5	94.3	0	-
<i>forgetting</i>	98.5	54.0	21.3	21.7	19.9	20.2	13.2	11.7	10.7	9.2	28.0	$\downarrow 66.3$	0
I3DOL [14]	98.1	97.0	93.4	91.1	89.7	88.2	83.5	77.8	73.1	61.5	85.3	$\downarrow 9.0$	800
InOR-Net [15]	98.1	<b>97.5</b>	<b>95.6</b>	<b>93.7</b>	91.4	90.3	85.9	79.2	74.6	63.9	87.0	$\downarrow 7.3$	800
<i>Memory Usage [14,15]</i>	<i>800</i>	<i>800</i>	<i>800</i>	<i>800</i>	<i>800</i>	<i>800</i>	<i>800</i>	<i>800</i>	<i>800</i>	<i>800</i>	-	-	-
Ours (Input features)	98.8	95.4	92.6	91.3	88.7	86.5	83.2	<u>81.7</u>	<u>79.8</u>	<u>76.7</u>	<u>87.5</u>	$\downarrow 6.8$	<b>400</b>
Ours (Local features)	98.8	95.9	93.3	92.4	89.8	88.3	85.6	83.8	81.1	78.3	88.7	$\downarrow 5.6$	<b>400</b>
Ours (Global features)	98.8	96.2	93.8	92.7	90.6	89.7	<u>86.7</u>	<u>85.6</u>	<u>83.2</u>	<u>79.1</u>	89.6	$\downarrow 4.7$	<b>400</b>
Ours (Fusion)	98.8	96.4	94.1	93.2	<b>91.5</b>	<b>90.7</b>	<b>87.1</b>	<b>86.3</b>	<b>85.1</b>	<b>80.8</b>	<b>90.4</b>	$\downarrow 3.9$	<b>400</b>
<i>Memory Usage (Ours)</i>	<i>40</i>	<i>80</i>	<i>120</i>	<i>160</i>	<i>200</i>	<i>240</i>	<i>280</i>	<i>320</i>	<i>360</i>	<i>400</i>	-	-	-

Table 1. Accuracy comparison on ModelNet40 Dataset [47] over 10 incremental stages. The final columns indicate the average accuracy across all stages (Avg.), the forgetting rate ( $\Delta\%$ ), and the total number of exemplars stored in memory (M). We also report the number of exemplars in memory (*Memory Usage*) for each stage. Additionally, "joint" refers to learning all classes together, while "forgetting" learns stages consecutively without preventing forgetting. The best results are highlighted in **bold**, and our improvements are underlined. Notice that the slightly lower performance of our approach in the initial stages is a result of significantly reduced memory usage, for instance, only utilizing one-tenth and one-fifth of InOR-net's memory in stages 2 and 4, respectively.

layer, while [46] involves learning a bias-correction model for post-processing output logits. In this work, we explore the use of *focal Loss* [26], initially introduced for object detection tasks. Our experiments indicate that this approach can serve as a novel yet effective solution in the context of continual learning. The focal loss [26] can be defined as

$$FL(p_t) = -\alpha_t (1 - p_t)^\gamma \log(p_t), \quad (4)$$

where  $p_t$  is the model's estimated probability for each class,  $\alpha_t$  is a balancing parameter to address class imbalance, and  $\gamma$  is a focusing parameter to steer the model's focus towards hard examples. By focusing on the harder examples from these new classes, the model can learn more effectively from limited data.

## 5. Experiments

### 5.1. Settings

We follow the experimental setup from I3DOL [14] and InOR-net [15], including the datasets, backbone, and number of incremental stages. To the best of our knowledge, these are the only works focused on exemplar-based continual learning for point clouds. Non-exemplar-based methods have reported significantly lower accuracy [23].

**Datasets.** We conduct tests on three datasets: ModelNet40 [47], ShapeNet [5], and ScanNet [11]. ModelNet40 [47] contains 40 distinct classes of clean 3D CAD models. Following [14] and [15], we establish a total of 10 incremental stages with every stage adding four new classes. We store 10 exemplars from each class, leading to an overall memory usage of 400 samples.

For the ShapeNet Dataset [5] we use 53 categories to be consistent with I3DOL [14] and InOR-net [15]. We follow their setting of 9 incremental stages with each stage introducing six new classes, except for the final stage which introduces five classes. There is no need for sample alignment in our procedures, as the ShapeNet dataset [5] already arrives in an aligned format.

The ScanNet dataset includes 17 different classes, all obtained from scanning real indoor scenes. Compared to ShapeNet [5] and ModelNet40 [47], ScanNet [11] presents a greater challenge for our framework due to its noisy geometric structures and lack of alignment. We apply the FilterReg [16] technique for aligning samples to compute a reliable distance matrix. Our model stores 10 samples per class, with a total of 9 incremental states each adding two new classes, apart from the final state adding just one.

**Implementation Details.** CL3D is implemented with PyTorch and trained on a Tesla V4 GPU with a batch size of 32. To maintain a fair comparison with previous studies [14, 15], we use PointNet [33] as our backbone. We choose the Adam optimizer and the cosine annealing learning rate schedule with an initial learning rate of  $10^{-3}$ . The number of epochs is set to 50 in incremental stages. We set the distillation factor to 0.1 for the knowledge distillation loss and choose  $\gamma = 2$  for the focal loss.

### 5.2. Comparison

We conduct comparative analyses with I3DOL [14] and InOR-net [15]. For a comprehensive perspective, we report the scenario where the network has access to the complete dataset from previous tasks (*joint training*) as an ideal upper

Incremental Stage	1	2	3	4	5	6	7	8	9	Avg.	$\Delta(\%)$	M
Number of Classes	6	12	18	24	30	36	42	48	53			
<i>joint</i>	98.0	97.3	95.4	94.4	92.8	91.6	90.9	90.5	89.3	93.3	0	-
<i>forgetting</i>	98.0	46.3	53.4	4.5	11.8	6.6	3.2	12.5	6.2	26.9	$\downarrow 66.4$	0
I3DOL [14]	97.5	94.4	90.2	84.3	80.5	76.1	73.5	70.8	67.3	81.6	$\downarrow 11.7$	1000
InOR-Net [15]	97.5	<b>95.6</b>	<b>92.4</b>	86.7	83.1	79.2	76.0	73.5	69.4	83.7	$\downarrow 9.6$	1000
<i>Memory Usage [14, 15]</i>	<i>1000</i>	<i>1000</i>	<i>1000</i>	<i>1000</i>	<i>1000</i>	<i>1000</i>	<i>1000</i>	<i>1000</i>	<i>1000</i>	-	-	-
Ours (Input features)	98.0	91.7	90.2	<u>86.9</u>	<u>84.2</u>	<u>80.1</u>	<u>77.4</u>	<u>74.1</u>	<u>69.6</u>	83.5	$\downarrow 9.8$	<b>530</b>
Ours (Local features)	98.0	91.6	90.3	<u>87.2</u>	<u>84.9</u>	<u>81.4</u>	<u>78.3</u>	<u>76.1</u>	<u>70.3</u>	84.2	$\downarrow 9.1$	<b>530</b>
Ours (Global features)	98.0	91.8	90.9	<u>87.8</u>	<u>85.7</u>	<u>82.6</u>	<u>80.2</u>	<u>77.5</u>	<u>71.3</u>	85.1	$\downarrow 8.2$	<b>530</b>
Ours (Fusion)	98.0	91.8	90.8	<b>88.2</b>	<b>86.5</b>	<b>83.4</b>	<b>81.5</b>	<b>78.6</b>	<b>72.4</b>	<b>85.7</b>	$\downarrow 7.6$	<b>530</b>
<i>Memory Usage (Ours)</i>	<i>60</i>	<i>120</i>	<i>180</i>	<i>240</i>	<i>300</i>	<i>360</i>	<i>420</i>	<i>480</i>	<i>530</i>	-	-	-

Table 2. Accuracy comparison on ShapeNet [5] over 9 incremental stages. Similar to Tab. 1, lower performance on stages 1 and 2 is due to extremely smaller memory usage compared to InOR-net.

bound. As a lower bound, we present the results of full forgetting (denoted as *forgetting* in the tables) where the model updates its parameters solely based on new tasks.

**Results on ModelNet40.** Tab. 1 demonstrates a comparison on the ModelNet40 dataset [47]. By integrating the spectral embeddings from input, local, and global features, our model achieves a 3.4% increase in average accuracy compared to InOR-net [15], while using substantially less memory in every stage. In the final stage, we achieve a remarkable 16.9% increase in accuracy compared to InOR-net, using only half the memory. It is notable that just using the input space features, we perform on par with the state of the art, enhancing average accuracy by 0.5%. We reiterate that using solely the input data removes any reliance on the network architecture. Additionally, note that the average accuracy also takes into account the initial stages where we use considerably less memory. The forgetting rate has decreased to 6.8% for the input approach and to 3.9% for the fused features.

**Results on ShapeNet.** Tab. 2 shows our result on the ShapeNet dataset [5], which has more classes than ModelNet [47] and ScanNet [11]. On this dataset, our fusion method achieved an accuracy increase of 2.0% compared to InOR-net [15], while using only 10 samples per class in memory. In the final stage, we beat InOR-net by 3.0% while using nearly half the memory. Our forgetting rate is 9.8% for input features and 7.6% for the fused features.

**Results on ScanNet.** The ScanNet dataset [11], as a real-world point cloud dataset, presents increased challenges due to its noisiness, incompleteness, and other complex characteristics. By utilizing 10 samples per class in our fusion approach, we achieve an increase of 4.1% in average accuracy over the state of the art. In the final stage, we obtain a

14.0% more accuracy while using only 28% of the memory used by InOR-net [15]. Our results illustrate that in real-world scenarios, proper selection of exemplars can make a significant difference and greatly affect learning in the next stages. The imperfect quality of point clouds increases the risk of selecting suboptimal samples.

### 5.3. Ablation Study

**The Effect of Focal Loss.** As discussed in Sec. 4.5 we have implemented *focal loss* [26] to address class imbalance. Fig. 4 clearly demonstrates the effectiveness of focal loss when using only the input space spectral features with 5 samples per class. The comparison with the *Cross-Entropy loss* highlights the significant impact of focal loss on maintaining model accuracy through the various stages of continual learning.

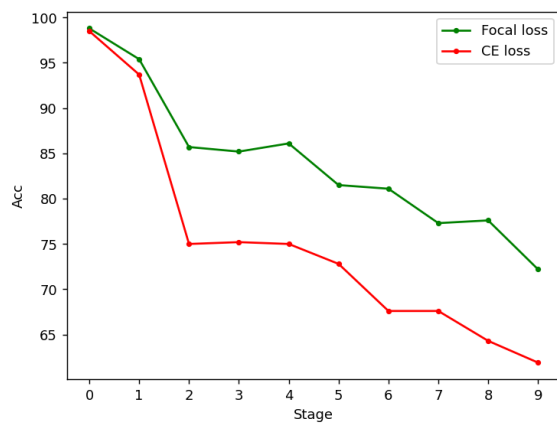


Figure 4. The effect of focal loss compared to Cross-Entropy loss on classification accuracy in a continual learning setting using input space spectral features with 5 samples per class on ModelNet40 [47]

Incremental Stage	1	2	3	4	5	6	7	8	9	Avg.	$\Delta(\%)$	M
Number of Classes	2	4	6	8	10	12	14	16	17			
<i>joint</i>	96.8	94.8	93.4	93.2	92.9	92.3	91.8	91.3	91.0	93.0	0	-
<i>forgetting</i>	95.6	49.8	32.5	23.7	20.2	13.8	15.0	12.3	8.2	30.1	$\downarrow 66.3$	0
I3DOL [14]	93.2	87.2	80.5	77.8	64.3	61.9	58.2	56.8	52.1	70.2	$\downarrow 22.8$	600
InOR-Net [15]	93.2	<b>88.7</b>	<b>82.6</b>	<b>79.4</b>	67.9	64.0	60.6	58.3	54.8	72.2	$\downarrow 20.8$	600
<i>Memory Usage [14, 15]</i>	600	600	600	600	600	600	600	600	600	-	-	-
Ours (Input features)	97.5	79.4	75.5	74.3	<u>73.1</u>	<u>71.7</u>	<u>70.2</u>	<u>67.2</u>	<u>63.4</u>	<u>74.6</u>	$\downarrow 18.4$	<b>170</b>
Ours (Local features)	97.5	78.7	75.2	74.5	<u>73.4</u>	<u>71.3</u>	<u>69.5</u>	<u>66.3</u>	<u>62.2</u>	<u>74.3</u>	$\downarrow 18.7$	<b>170</b>
Ours (Global features)	97.5	79.3	75.8	75.1	<u>74.2</u>	<b>73.3</b>	<u>71.5</u>	<u>69.6</u>	<u>65.1</u>	<u>75.7</u>	$\downarrow 17.3$	<b>170</b>
Ours (Fusion)	97.5	78.8	75.6	75.3	<b>74.5</b>	<u>73.1</u>	<b>72.2</b>	<b>71.4</b>	<b>68.8</b>	<b>76.3</b>	$\downarrow 16.7$	<b>170</b>
<i>Memory Usage (Ours)</i>	20	40	60	80	100	120	140	160	170	-	-	-

Table 3. Performance comparison on ScanNet dataset [11] over 9 incremental stages. As in Tab. 1 and Tab. 2, the lower performance in the initial stages is due to significantly reduced memory usage compared to InOR-net utilizing just 7%, 10%, and 14% for stages 2, 3, and 4, respectively.

### Replace Clustering with Herding or Random Selection.

To assess whether our approach’s success is due to clustering or other factors like distillation or focal loss, we replaced the clustering-based exemplar selection with herding [36] or random selection, keeping all other components unchanged. The results, depicted in Fig. 5, clearly indicate that clustering indeed plays a significant role in boosting our method’s performance.

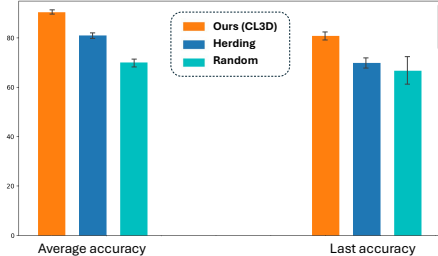


Figure 5. Comparing clustering-based exemplar selection with *herding* and random selection, reporting the *average accuracy* (left) and the accuracy in the last stage (right) on ModelNet [47].

**Feature Fusion.** It is natural to question whether incorporating all three types of features—input, local, and global—truly enhances the overall accuracy. Tab. 4 presents accuracy metrics for various combinations of these features. The data clearly indicate that combining input, local, and global features leads to superior performance compared to utilizing them individually or in pairs.

## 6. Discussion

Our CL3D model demonstrates strong performance but faces challenges. The current exemplar selection method, based on choosing  $K$  clusters, results in a linear increase in memory usage, limiting our ability to maintain a fixed memory budget. A transition to hierarchical clustering

Input	Local	Global	$ACC_{avg}$	$ACC_{last}$
✓			87.8	76.7
✓	✓		88.5	77.4
	✓		88.7	78.3
✓		✓	88.8	78.8
		✓	89.6	79.1
	✓	✓	89.7	79.5
✓	✓	✓	<b>90.4</b>	<b>80.8</b>

Table 4. Accuracy comparison on ModelNet40 [47] with 10 samples per class, using different combinations of input, local, and global features. The table shows the average accuracy ( $ACC_{avg}$ ) and the accuracy at the last stage ( $ACC_{last}$ ). Combining all three features (Input, Local, Global) achieves the highest average accuracy (90.4%) and last accuracy (80.8%)

could allow for a more adaptive exemplar selection across stages. Additionally, the most computationally expensive step is computing the affinity between all point cloud samples within a class, leading to quadratic complexity. Fortunately, this issue has been addressed extensively in the context of spectral clustering [3, 6, 21].

## 7. Conclusion

In this paper, we introduce CL3D, a novel framework for continual learning in 3D point cloud objects. By leveraging spectral clustering in input, local, and global feature spaces, we effectively identify key exemplars for continual learning. Our approach is backbone-independent in the input section, making it adaptable for future methods. Extensive experiments on ModelNet40, ShapeNet, and ScanNet demonstrate that CL3D achieves superior accuracy with reduced memory requirements compared to existing 3D methods.



## References

- [1] Rahaf Aljundi, Francesca Babiloni, Mohamed Elhoseiny, Marcus Rohrbach, and Tinne Tuytelaars. Memory aware synapses: Learning what (not) to forget. In *Proceedings of the European Conference on Computer Vision (ECCV)*, September 2018. [2](#)
- [2] Paul J Besl and Neil D McKay. Method for registration of 3-d shapes. In *Sensor fusion IV: control paradigms and data structures*, volume 1611, pages 586–606. Spie, 1992. [4](#)
- [3] Christos Boutsidis and Petros Drineas. Random projections for the nonnegative least-squares problem. *Linear algebra and its applications*, 431(5-7):760–771, 2009. [8](#)
- [4] Francisco M. Castro, Manuel J. Marin-Jimenez, Nicolas Guil, Cordelia Schmid, and Karteek Alahari. End-to-end incremental learning. In *Proceedings of the European Conference on Computer Vision (ECCV)*, September 2018. [2](#)
- [5] A. X. Chang, T. A. Funkhouser, L. J. Guibas, P. Hanrahan, Q. Huang, Z. Li, S. Savarese, M. Savva, S. Song, H. Su, J. Xiao, L. Yi, and F. Yu. Shapenet: An information-rich 3d model repository. *arXiv preprint arXiv:1512.03012*, 2015. [2](#), [6](#), [7](#)
- [6] Fowlkes Charless. Spectral grouping using the nystrom method. *IEEE Trans. PAMI*, 2004. [8](#)
- [7] Arslan Chaudhry, Puneet K. Dokania, Thalaiyasingam Ajanthan, and Philip H. S. Torr. Riemannian walk for incremental learning: Understanding forgetting and intransigence. In *Proceedings of the European Conference on Computer Vision (ECCV)*, September 2018. [2](#)
- [8] Ali Cheraghian, Shafin Rahman, Dylan Campbell, and Lars Petersson. Transductive zero-shot learning for 3d point cloud classification. In *Proceedings of the IEEE/CVF winter conference on applications of computer vision*, pages 923–933, 2020. [1](#)
- [9] Townim Chowdhury, Ali Cheraghian, Sameera Ramasinghe, Sahar Ahmadi, Morteza Saberi, and Shafin Rahman. Few-shot class-incremental learning for 3d point cloud objects. In *European Conference on Computer Vision*, pages 204–220. Springer, 2022. [2](#)
- [10] Townim Chowdhury, Mahira Jalisha, Ali Cheraghian, and Shafin Rahman. Learning without forgetting for 3d point cloud objects. In *Advances in Computational Intelligence: 16th International Work-Conference on Artificial Neural Networks, IWANN 2021, Virtual Event, June 16–18, 2021, Proceedings, Part I 16*, pages 484–497. Springer, 2021. [2](#), [3](#)
- [11] Angela Dai, Angel X. Chang, Manolis Savva, Maciej Halber, Thomas Funkhouser, and Matthias Nießner. Scannet: Richly-annotated 3d reconstructions of indoor scenes. In *Proc. Computer Vision and Pattern Recognition (CVPR)*, IEEE, 2017. [2](#), [6](#), [7](#), [8](#)
- [12] Jia Deng, Wei Dong, Richard Socher, Li-Jia Li, Kai Li, and Li Fei-Fei. Imagenet: A large-scale hierarchical image database. In *2009 IEEE conference on computer vision and pattern recognition*, pages 248–255. Ieee, 2009. [1](#)
- [13] Prithviraj Dhar, Rajat Vikram Singh, Kuan-Chuan Peng, Ziyang Wu, and Rama Chellappa. Learning without memorizing. In *Proceedings of the IEEE/CVF Conference on Computer Vision and Pattern Recognition (CVPR)*, June 2019. [2](#)
- [14] Jiahua Dong, Yang Cong, Gan Sun, Bingtao Ma, and Lichen Wang. I3dol: Incremental 3d object learning without catastrophic forgetting. In *Proceedings of the AAAI Conference on Artificial Intelligence*, volume 35, pages 6066–6074, 2021. [2](#), [6](#), [7](#), [8](#)
- [15] Jiahua Dong, Yang Cong, Gan Sun, Lixu Wang, Lingjuan Lyu, Jun Li, and Ender Konukoglu. Inor-net: Incremental 3-d object recognition network for point cloud representation. *IEEE Transactions on Neural Networks and Learning Systems*, 2023. [2](#), [6](#), [7](#), [8](#)
- [16] Wei Gao and Russ Tedrake. Filterreg: Robust and efficient probabilistic point-set registration using gaussian filter and twist parameterization. In *Proceedings of the IEEE/CVF conference on computer vision and pattern recognition*, pages 11095–11104, 2019. [4](#), [6](#)
- [17] Ankit Goyal, Hei Law, Bowei Liu, Alejandro Newell, and Jia Deng. Revisiting point cloud shape classification with a simple and effective baseline. In *International Conference on Machine Learning*, pages 3809–3820. PMLR, 2021. [2](#)
- [18] Yulan Guo, Hanyun Wang, Qingyong Hu, Hao Liu, Li Liu, and Mohammed Bennamoun. Deep learning for 3d point clouds: A survey. *IEEE transactions on pattern analysis and machine intelligence*, 43(12):4338–4364, 2020. [1](#)
- [19] Geoffrey Hinton, Oriol Vinyals, and Jeff Dean. Distilling the knowledge in a neural network. In *NIPS Deep Learning and Representation Learning Workshop*, 2015. [2](#)
- [20] Saihui Hou, Xinyu Pan, Chen Change Loy, Zilei Wang, and Dahua Lin. Learning a unified classifier incrementally via rebalancing. In *Proceedings of the IEEE/CVF Conference on Computer Vision and Pattern Recognition (CVPR)*, June 2019. [2](#)
- [21] Dong Huang, Chang-Dong Wang, Jian-Sheng Wu, Jian-Huang Lai, and Chee-Keong Kwoh. Ultra-scalable spectral clustering and ensemble clustering. *IEEE Transactions on Knowledge and Data Engineering*, 32(6):1212–1226, 2019. [8](#)
- [22] Ronald Kemker, Marc McClure, Angelina Abitino, Tyler Hayes, and Christopher Kanan. Measuring catastrophic forgetting in neural networks. In *Proceedings of the AAAI conference on artificial intelligence*, volume 32, 2018. [1](#)
- [23] Shivanand Kundargi, Tejas Anvekar, Ramesh Ashok Tabib, and Uma Mudenagudi. Pointclimb: An exemplar-free point cloud class incremental benchmark. *arXiv preprint arXiv:2304.06775*, 2023. [6](#)
- [24] Felix Järemo Lawin, Martin Danelljan, Patrik Tostberg, Goutam Bhat, Fahad Shahbaz Khan, and Michael Felsberg. Deep projective 3d semantic segmentation. In *Computer Analysis of Images and Patterns: 17th International Conference, CAIP 2017, Ystad, Sweden, August 22-24, 2017, Proceedings, Part I 17*, pages 95–107. Springer, 2017. [2](#)
- [25] Zhizhong Li and Derek Hoiem. Learning without forgetting. *IEEE transactions on pattern analysis and machine intelligence*, 40(12):2935–2947, 2017. [2](#)
- [26] Tsung-Yi Lin, Priya Goyal, Ross Girshick, Kaiming He, and Piotr Dollar. Focal loss for dense object detection. In *Proceedings of the IEEE International Conference on Computer Vision (ICCV)*, Oct 2017. [6](#), [7](#)

- [27] Arun Mallya, Dillon Davis, and Svetlana Lazebnik. Piggyback: Adapting a single network to multiple tasks by learning to mask weights. In *Proceedings of the European Conference on Computer Vision (ECCV)*, September 2018. 2
- [28] Arun Mallya and Svetlana Lazebnik. Packnet: Adding multiple tasks to a single network by iterative pruning. In *Proceedings of the IEEE Conference on Computer Vision and Pattern Recognition (CVPR)*, June 2018. 2
- [29] Marc Masana, Xialei Liu, Bartłomiej Twardowski, Mikel Menta, Andrew D Bagdanov, and Joost Van De Weijer. Class-incremental learning: survey and performance evaluation on image classification. *IEEE Transactions on Pattern Analysis and Machine Intelligence*, 45(5):5513–5533, 2022. 4
- [30] Michael McCloskey and Neal J. Cohen. Catastrophic interference in connectionist networks: The sequential learning problem. volume 24 of *Psychology of Learning and Motivation*, pages 109–165. Academic Press, 1989. 2
- [31] Andrew Y. Ng, Michael I. Jordan, and Yair Weiss. On spectral clustering: Analysis and an algorithm. In *ADVANCES IN NEURAL INFORMATION PROCESSING SYSTEMS*, pages 849–856. MIT Press, 2001. 3
- [32] Oleksiy Ostapenko, Mihai Puscas, Tassilo Klein, Patrick Jahnichen, and Moin Nabi. Learning to remember: A synaptic plasticity driven framework for continual learning. In *Proceedings of the IEEE/CVF Conference on Computer Vision and Pattern Recognition (CVPR)*, June 2019. 2
- [33] Charles R Qi, Hao Su, Kaichun Mo, and Leonidas J Guibas. Pointnet: Deep learning on point sets for 3d classification and segmentation. In *Proceedings of the IEEE conference on computer vision and pattern recognition*, pages 652–660, 2017. 1, 2, 3, 4, 6
- [34] Charles Ruizhongtai Qi, Li Yi, Hao Su, and Leonidas J Guibas. Pointnet++: Deep hierarchical feature learning on point sets in a metric space. In I. Guyon, U. Von Luxburg, S. Bengio, H. Wallach, R. Fergus, S. Vishwanathan, and R. Garnett, editors, *Advances in Neural Information Processing Systems*, volume 30. Curran Associates, Inc., 2017. 1, 2
- [35] Shi Qiu, Saeed Anwar, and Nick Barnes. Geometric back-projection network for point cloud classification. *IEEE Transactions on Multimedia*, 24:1943–1955, 2021. 2
- [36] Sylvestre-Alvise Rebuffi, Alexander Kolesnikov, Georg Sperl, and Christoph H. Lampert. icarl: Incremental classifier and representation learning. In *Proceedings of the IEEE Conference on Computer Vision and Pattern Recognition (CVPR)*, July 2017. 1, 2, 3, 8
- [37] Andrei A Rusu, Neil C Rabinowitz, Guillaume Desjardins, Hubert Soyer, James Kirkpatrick, Koray Kavukcuoglu, Razvan Pascanu, and Raia Hadsell. Progressive neural networks. *arXiv preprint arXiv:1606.04671*, 2016. 2
- [38] Radu Bogdan Rusu, Nico Blodow, and Michael Beetz. Fast point feature histograms (fpfh) for 3d registration. In *2009 IEEE international conference on robotics and automation*, pages 3212–3217. IEEE, 2009. 4
- [39] Weijing Shi and Raj Rajkumar. Point-gnn: Graph neural network for 3d object detection in a point cloud. In *Proceedings of the IEEE/CVF conference on computer vision and pattern recognition*, pages 1711–1719, 2020. 1
- [40] Hanul Shin, Jung Kwon Lee, Jaehong Kim, and Jiwon Kim. Continual learning with deep generative replay. *Advances in neural information processing systems*, 30, 2017. 2
- [41] Christian Simon, Piotr Koniusz, and Mehrtaf Harandi. On learning the geodesic path for incremental learning. In *Proceedings of the IEEE/CVF Conference on Computer Vision and Pattern Recognition (CVPR)*, pages 1591–1600, June 2021. 5
- [42] Ulrike von Luxburg. A tutorial on spectral clustering. *Statistics and Computing*, 17(4):395–416, 2007. 3
- [43] Yue Wang, Yongbin Sun, Ziwei Liu, Sanjay E Sarma, Michael M Bronstein, and Justin M Solomon. Dynamic graph cnn for learning on point clouds. *ACM Transactions on Graphics (tog)*, 38(5):1–12, 2019. 1, 2
- [44] Chenshen Wu, Luis Herranz, Xialei Liu, Joost Van De Weijer, Bogdan Raducanu, et al. Memory replay gans: Learning to generate new categories without forgetting. *Advances in Neural Information Processing Systems*, 31, 2018. 2
- [45] Tong Wu, Liang Pan, Junzhe Zhang, Tai Wang, Ziwei Liu, and Dahua Lin. Density-aware chamfer distance as a comprehensive metric for point cloud completion. *arXiv preprint arXiv:2111.12702*, 2021. 3
- [46] Yue Wu, Yinpeng Chen, Lijuan Wang, Yuancheng Ye, Zicheng Liu, Yandong Guo, and Yun Fu. Large scale incremental learning. In *Proceedings of the IEEE/CVF Conference on Computer Vision and Pattern Recognition (CVPR)*, June 2019. 6
- [47] Zhirong Wu, Shuran Song, Aditya Khosla, Fisher Yu, Linguang Zhang, Xiaoou Tang, and Jianxiong Xiao. 3d shapenets: A deep representation for volumetric shapes. *Proceedings of the 28th IEEE Conference on Computer Vision and Pattern Recognition (CVPR)*, 2015. 1, 2, 4, 6, 7, 8
- [48] Tiange Xiang, Chaoyi Zhang, Yang Song, Jianhui Yu, and Weidong Cai. Walk in the cloud: Learning curves for point clouds shape analysis. In *Proceedings of the IEEE/CVF International Conference on Computer Vision (ICCV)*, pages 915–924, October 2021. 2
- [49] Aoran Xiao, Xiaoqin Zhang, Ling Shao, and Shijian Lu. A survey of label-efficient deep learning for 3d point clouds. *IEEE Transactions on Pattern Analysis and Machine Intelligence*, 2024. 1
- [50] Mutian Xu, Junhao Zhang, Zhipeng Zhou, Mingye Xu, Xiaojuan Qi, and Yu Qiao. Learning geometry-disentangled representation for complementary understanding of 3d object point cloud. In *Proceedings of the AAAI conference on artificial intelligence*, volume 35, pages 3056–3064, 2021. 2
- [51] Yaoqing Yang, Chen Feng, Yiru Shen, and Dong Tian. Foldingnet: Point cloud auto-encoder via deep grid deformation. In *Proceedings of the IEEE conference on computer vision and pattern recognition*, pages 206–215, 2018. 1
- [52] Chuanguan Ye, Hongyuan Zhu, Bo Zhang, and Tao Chen. A closer look at few-shot 3d point cloud classification. *International Journal of Computer Vision*, 131(3):772–795, 2023. 1
- [53] Maciej Zamorski, Michał Stypułkowski, Konrad Karanowski, Tomasz Trzciniński, and Maciej Zieba. Continual learning on 3d point clouds with random compressed

- rehearsal. *Computer Vision and Image Understanding*, 228:103621, 2023. 2
- [54] Friedemann Zenke, Ben Poole, and Surya Ganguli. Continual learning through synaptic intelligence. In *International conference on machine learning*, pages 3987–3995. PMLR, 2017. 2
- [55] Na Zhao and Gim Hee Lee. Static-dynamic co-teaching for class-incremental 3d object detection. In *Proceedings of the AAAI Conference on Artificial Intelligence*, volume 36, pages 3436–3445, 2022. 2
- [56] Da-Wei Zhou, Qi-Wei Wang, Zhi-Hong Qi, Han-Jia Ye, De-Chuan Zhan, and Ziwei Liu. Deep class-incremental learning: A survey. *arXiv preprint arXiv:2302.03648*, 2023. 4